Dual-functional mesh with Zn-Ni-Co LDHs@NiMoO$_4$ heterojunction nanoarrays for highly efficient oil/water separation and photocatalytic degradation

Yongli Sun, Jingshuai Li, Luhong Zhang, Bin Jiang, Xiaodong Yang, Na Yang, Feifei Peng, Mi Xu, Xiaoming Xiao [*]

School of Chemical Engineering and Technology, Tianjin University, Tianjin 300072, People's Republic of China

ARTICLE INFO

ABSTRACT

In view of the serious water pollution issue, a kind of environmentally friendly, dual-functional, energy-efficient and low-cost superwetting material is urgently prepared for oil/water separation and the degradation of dyes in wastewater. In our work, dual-functional Zn-Ni-Co LDH@NiMoO$_4$ nanoarrays (ZNC-NM) with porous core-shell structure were constructed on the stainless steel mesh (SSM) via a facile two-step hydrothermal method. The coated mesh exhibited favorable superhydyophilicity and underwater superoleophobicity with underwater oil contact angle (OCA) of 164.9°. Meanwhile, the as-prepared mesh possessed ultrahigh separation efficiency and high permeation flux for a series of oil/water mixtures. In addition, the good anti-fouling and self-cleaning property enabled the separation efficiency remain above 99.90% after 60 separation recycles. By virtue of good stability and anti-corrosive property, there were no remarkable alterations in the separation efficiency and underwater OCA of the designed mesh in harsh environments. More importantly, the NiMoO$_4$ nanosheets anchored on Zn-Ni-Co LDH with the visible light responsiveness demonstrated favorable photocatalytic performance, which could efficiently degrade organic dyes in wastewater. Therefore, the dual-functional mesh coated with ZNC-NM nanoarrays based on this facile strategy is a promising material for oil/water separation and photocatalysis, owning great application potential in wastewater remediation.

1. Introduction

Oily water from oil exploitation, leakage of offshore crude oil industrial, and discharge of wastewater have been one of the most serious environmental issue, which cause irreversible damage to human health and environment [1–4]. Although kinds of strategies such as centrifugation [5], demulsifier [6] and microbial degradation [7] are implemented to separate oil and organic solvents from oily wastewater, these methods are still limited by high operational costs, poor resistance to pollution and low separation efficiency. Fortunately, superwetting materials inspired by lotus leaf [8] and fish scale [9] in nature have attracted considerable attention. Up to now, various materials have been used to synthesize superhydrophilic and superhydrophobic coatings for oil/water separation, such as LDH coating [10–12], polymer film [13–15], metal oxide film [16,17], etc. Compared with the tedious preparation process of polymer film, the inorganic coatings are drawing more attentions due to its environment adaptability, stability and excellent anti-fouling property. Therefore, it's significant to synthesis a novel material with a facile method for oil/water separation.

As a typical representation of two dimensional materials, the layered double hydroxides (LDHs) have received extensive research in various fields, such as electric catalytic [18], oil/water separation [11,19], photocatalytic degradation [20–22], etc. Various LDHs can be frequently fabricated by means of hydrothermal process, co-precipitation, crystallization isolation and anion-exchange [23–26]. Xie et al. [27] synthesized MgAlZn layered double hydroxide-coated stainless steel mesh with excellent superhydrophilicity, thus endowing ultrafast separation of oil/water mixtures. Lv et al. [28] utilizing the inherent hydrophilicity of LDH nanoscrolls successfully fabricated 3D multiscale superhydrophilic sponges with high-efficient separation for target oil/water mixtures, in which the delicately designed pore size was regulated with SiO$_2$ nanofibers. Although remarkable advance has been acquired in the field of oil/water separation, there are rare literatures on the applications of 1D LDH nanowires.

Molybdate, an inorganic functional material, has been widely researched for its peculiar physicochemical properties. In recent years, there have been a large number of reports on the optical, electrical and magnetic catalytic properties of molybdate [29–31], but few works targeted at the superwettability. It is known that surface microstructure and chemical composition are two important factors to realize superhydrophilicity or superhydrophobicity. The inherent hydrophilicity of the binary metal oxide $NiMoO_4$ provides a great possibility for the preparation of superhydrophilic materials. Meanwhile, molybdate with different micro morphologies can be prepared by controlling the reaction conditions. For instance, Peng et al. [32] constructed $NiMoO_4$ hierarchical architectures composed of nanosheet or nanorod arrays on various substrates by simply tuning the composition of solvents. Additionally, $NiMoO_4$ with the appropriate band gap (2.8 eV) shows great photocatalytic potential in degrading organic dyes on utilizing visible light from solar spectrum, thus contributing to the fabrication of multifunctional material [33–35]. Nevertheless, $NiMoO_4$ is rarely used as a photocatalyst alone in previous research due to lower photocatalytic performance caused by the high recombination rate of electron-hole pairs. To overcome the above problem, several approaches are applied to enhance the photocatalytic performance, especially the designation of heterojunction architecture photocatalytic systems with the advantages of fast charge transfer to the surface, effective charge separation, higher lifetime of the charge carriers and separation of locally adverse oxidation/reduction reactions in nanospace [34,36]. Based on the aforementioned analysis, we envisage that the formation of core-shell heterostructure between $NiMoO_4$ and LDH nanoarrays is feasible for the enhancement of photocatalytic performance and underwater superoleophobicity.

Herein, inorganic dual-functional ZNC@NM heterojunction nanoarrays were constructed on SSM (ZNC@NM-SSM) with a simple two-step hydrothermal method. To the best of our knowledge, the superwettability of $NiMoO_4$ was studied for the first time, and our coated mesh showed good underwater superoleophobicity with the underwater OCA of 164.9° after $NiMoO_4$ nanosheets were anchored on the Zn-Ni-Co nanowires. More significantly, the as-prepared heterojunction nanoarrays coated mesh not only realize the separation of oily wastewater with ultrahigh efficiency and high permeation flux, but also utilize its favorable photocatalytic performance to further purify organic dyes in wastewater. By virtue of the anti-corrosive performance, outstanding stability, self-cleaning and anti-fouling property, the ZNC@NM-SSM can maintain high separation efficiency and long lifespan, even treated in various harsh conditions. As a result, dual-functional low-cost inorganic coated mesh with ultrahigh efficiency, photocatalytic performance, reusability and stability exhibited great application prospect in oil/water separation and photocatalytic degradation.

2. Experimental

2.1. Materials and chemicals

The 316L Stainless steel meshes (SSMs: 2000 mesh size) were purchased from the local market (Tianjin, China). Hydrochloric acid (HCl, 35%) was obtained from Leon Lombard Pharmaceutical Chemical Co. Ltd (Tianjin, China). Cobalt nitrate hexahydrate ($Co(NO_3)_2·6H_2O$, AR) was purchased from Tianjin Komiou Chemical Reagent Co. Ltd (Tianjin, China). Nickel nitrate hexahydrate ($Ni(NO_3)_2·6H_2O$, AR) was purchased from Shanghai Titan Scientific Co., Ltd (Shanghai, China). Urea (CO $(NH_2)_2$, AR) and Zinc nitrate hexahydrate ($Zn(NO_3)_2·6H_2O$, AR) were obtained from the Shanghai Aladdin Biochemical Technology Co. Ltd. Sodium molybdate dihydrate ($Na_2MoO_4·2H_2O$, 98%) was obtained from Tianjin Heowns Biochemical Technology Co. Ltd (Tianjin, China). Deionized water was used in all experiments. All chemicals and reagents were used directly without further purification.

2.2. Synthesis of Zn-Ni-Co LDHs coated SSM

A piece of SSM with a size of $3 \times 3\ cm^2$ was sequentially ultrasonically washed with acetone, ethanol, deionized water for each 15 min at ambient to remove organic impurity. Afterwards, the processed mesh was immersed in an ultrasound bath of HCl solution (HCl: H_2O = 1:1, V/V) for 15 min to accomplish the etching procedure and rinsed with deionized water for several times. The hydrophilic layer of Zn-Ni-Co LDH nanowires was obtained by a symbol hydrothermal process similar to previous report [37]. Simply, 2 mmol of $Co(NO_3)_2·6H_2O$, 1 mmol of $Ni(NO_3)_2·6H_2O$, 1 mmol of $Zn(NO_3)_2·6H_2O$, 6 mmol of CO $(NH_2)_2$ and 1 mmol of NH_4F were mixed with 80 ml of deionized water under vigorous magnetic stirring for 30 min to form a clear pink solution. Then the etched SSM was vertically placed in a 100 ml Teflon-lined autoclave containing solution at 120 °C for 8 h to get Zn-Ni-Co LDH nanowires coated mesh (ZNC-SSM). After the hydrothermal reaction, the ZNC-SSM was washed with ethanol and deionized water and dried in vacuum oven at 80 °C.

2.3. Preparation of ZNC@NM-SSM

To fabricate Zn-Ni-Co LDHs@$NiMoO_4$ heterostructure nanoarrays coated mesh, the typical hydrothermal process was adopted to fabricate $NiMoO_4$ nanosheets which were anchored on the Zn-Ni-Co LDHs nanowires. The obtained ZNC-SSM was placed vertically in the prepared 80 ml solution containing 1 mmol $Ni(NO_3)_2·6H_2O$ and 1 mmol $Na_2MoO_4·2H_2O$ in autoclave at 100 °C for 12 h. After cooling to room temperature, the ZNC@NM-SSM was taken out and then washed with deionized water for several times to remove impurities. Finally, the obtained mesh was dried for later use and characterization.

2.4. Characterization

Scanning electron microscopy (SEM) combined with energy dispersive spectrometer (EDS) was conducted using a field-emission scanning electron microscope (Hitachi S-4800, Japan) for surface morphology observation and the exploration of elements distribution of original mesh, ZNC-SSM and ZNC@NM-SSM. The X-ray photoelectron spectra (XPS) was conducted on the element composition of ZNC@NM heterostructure nanoarrays. Moreover, crystal structure of the as-synthesized material was confirmed by X-ray diffraction (XRD, D8-Focus, AXS, Germany) with Cu Kα radiation in the 2θ range 5–80° and the scanning rate was 3°/min.

To measure water contact angle (WCA) and the diffusion process of water, the water droplet was directly dropped on the surface of ZNC@NM-SSM and captured data with a high speed camera. In addition, an optical contact angle and an interface meter (SL200 KS, KINO, USA) were adopted to measure the underwater OCA by dropping the various kinds of oil droplets with 4–8 μl on the coating mesh immersed in water at ambient temperature. All the contact angles were acquired by averaging five measurement of a sample. The ultraviolet–visible (UV–vis) absorption of the dye solutions were measured with a UV–vis spectrophotometer (UV-4802S, Unico, USA).

2.5. Oil/water separation experiment

Two different devices, vertical and inclined devices were respectively utilized to complete the separation experiment of light oils and heavy oils, respectively. The ZNC@NM-SSM coated mesh with diameter of 1.8 cm was sandwiched between two flanges connected with glass tube. Five light oils containing isooctane, petroleum, n-hexane, kerosene, diesel and a heavy oil of dichloromethane were selected as model oils. When 140 ml of mixtures of oil (dyed with oil red) and water phase (1:1 V/V) were poured into the filter-separation device, the water phase could penetrate through the mesh, but the oil was intercepted due to the superhydrophilicity of the ZNC@NM-SSM. The oil content in the

filtrates was extracted by CCl₄ and then measured by an infrared oil content analyzer (F2000, China). For the separation experiment of emulsified oily wastewater, the oil-in-water emulsions were prepared by adding 10 g oil in 1000 ml distillation water under sharply stirring with a homogenizer (Fluke homogenizer, FA25, 500 W) at 10,000 rpm for 5 min. The separation efficiency (η) can be calculated with the following Eq. (1).

$$\eta = (1 - \frac{C}{C_0}) \times 100\% \tag{1}$$

where C_0 and C represent the mass concentration of oil phase before and after filtration, respectively.

The separation flux was calculated by the Eq. (2).

$$F = \frac{V}{S \times t} \tag{2}$$

where V represents the volume of water phase that permeates through the coated mesh, S is the effective filtration area and t is the filtering time.

2.6. Photocatalytic degradation experiment

Photocatalytic degradation experiment is conducted in an experimental box, in which there is a long arc xenon light source. The xenon lamp is connected with condensed circulating water to maintain a constant temperature. As common dyes in industrial wastewater, Congo red (CR) and Methyl blue (MB) are selected as samples to evaluate the photocatalytic degradation capability of the ZNC@NM-SSM. The as-prepared coated mesh with a size of 1.5 × 1.5 cm² was placed in a glass vessel containing 20 ml organic dye solution (30 ppm) under darkness to complete the adsorption process and then vessel was transformed to experimental box irradiated with visible light to perform the degradation experiment. During the degradation process, the UV absorption characteristics of MB solution and CR solution at 591.5 nm and 501 nm are monitored at certain intervals of time, respectively, to evaluate degradation ability of coated mesh. The photocatalytic efficiency is calculated by Eq. (3).

$$\eta = (1 - \frac{C_i}{C_0}) \times 100\% \tag{3}$$

where C_0 and C_i are the dye concentration before irradiation and after irradiation at different times, respectively.

3. Results and discussion

3.1. Characterization and surface morphology

The ZNC@NM heterostructure nanoarrays coated SSM was fabricated with simple two-step hydrothermal reaction (as illustrated in Fig. 1). Initially, the SSM etched with HCl solution not only removed the metal oxides on the surface, but also formed a rough structure, which was beneficial to the adhesion of the metal ions. Subsequently, as the hydrothermal temperature gradually rose, the metal ions attached on the surface formed 1D ZNC LDHs nanowires in alkaline environment resulted from the decomposition of urea. Subsequently, interconnected NiMoO₄ nanosheets were deposited on the tightly arranged nanowires via a secondary hydrothermal process. The construction of ZNC@NM heterojunction nanoarrays on the SSM endowed the coated mesh favorable superhydrophilic and photocatalytic properties.

The surface morphology of the original SSM, ZNC-SSM and ZNC@NM-SSM was explored by SEM. As was shown in Fig. 2a-c, the surface of bare SSM was extremely smooth with the grid pore diameter of approximate 10–20 μm, which was not conductive to the construction of nanoarrays. Therefore, the strategy of etching SSM with hydrochloric acid solution was adopted to change the roughness of SSM. It could be seen from Fig. 2d-f that the linear ternary ZNC LDHs were grown on the surface of SSM compactly, and nanowires were around 1–4 μm in length. It was worth noting that ZNC nanowires and ZNC@NM nanoarrays on the SSM were divided into regular distribution and irregular distribution. As shown in Fig. S1, most of ZNC LDHs nanowires were regularly distributed and only a small minority of ZNC LDHs nanowires were irregularly distributed on part surface of the SSM which was probably resulted by the easy deposition on the upper layer of the nanowires on part surface of the SSM of the redundant Zn-Ni-Co LDH crystals grown in the aqueous solution. After wrapping the ZNC LDH nanowires with ultrathin NiMoO₄ nanosheets (Fig. 2g-i), seagrass-like ZNC@NM heterojunction nanoarrays with high roughness and surface area were obtained. To further determine the composition of ZNC@NM heterojunction nanoarrays, an energy dispersive spectrometer was used to verify the existence of Zn, Ni, Co Mo, O. Fig. S2 showed the EDS results of the ZNC@NM, which indicated the component of heterojunction nanoarrays and the content of each element. In the mapping image (Fig. 2j-o), it could be obviously observed that five elements were homogeneously distributed on the surface of SSM, which demonstrated the successful construction of ZNC@NM heterojunction nanoarrays.

The crystalline phase of the fabricated ZNC@NM at each hydrothermal step was explored by XRD. Considering the strong impact of the
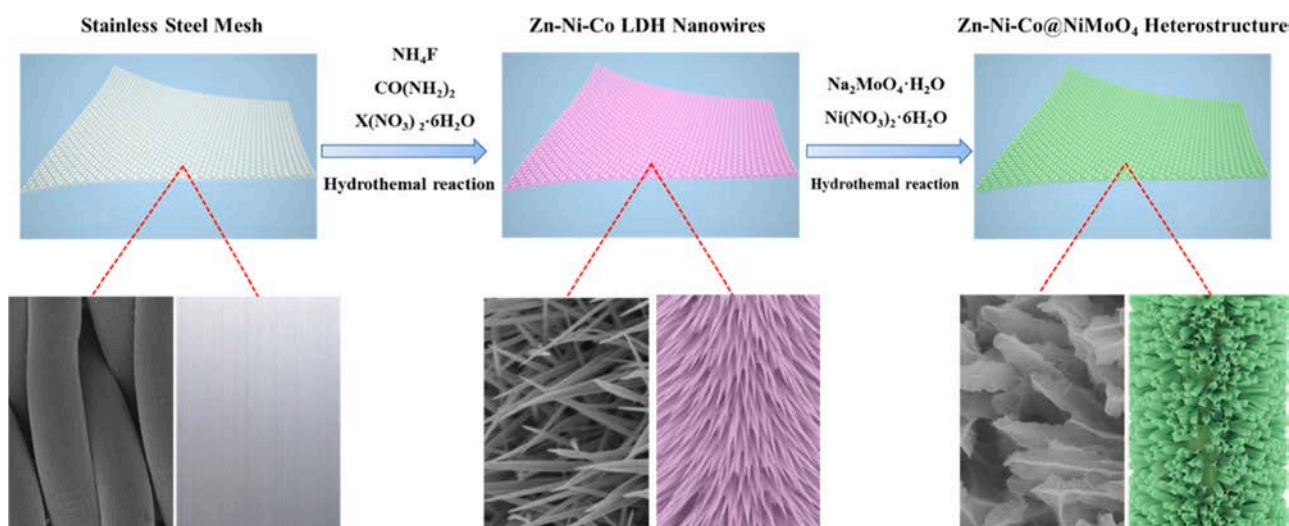

Fig. 1. Schematic illustration of designed processes of ZNC@NM-SSM, X(NO₃)₂·6H₂O contains Co(NO₃)₂·6H₂O, Ni(NO₃)₂·6H₂O and Zn(NO₃)₂·6H₂O.
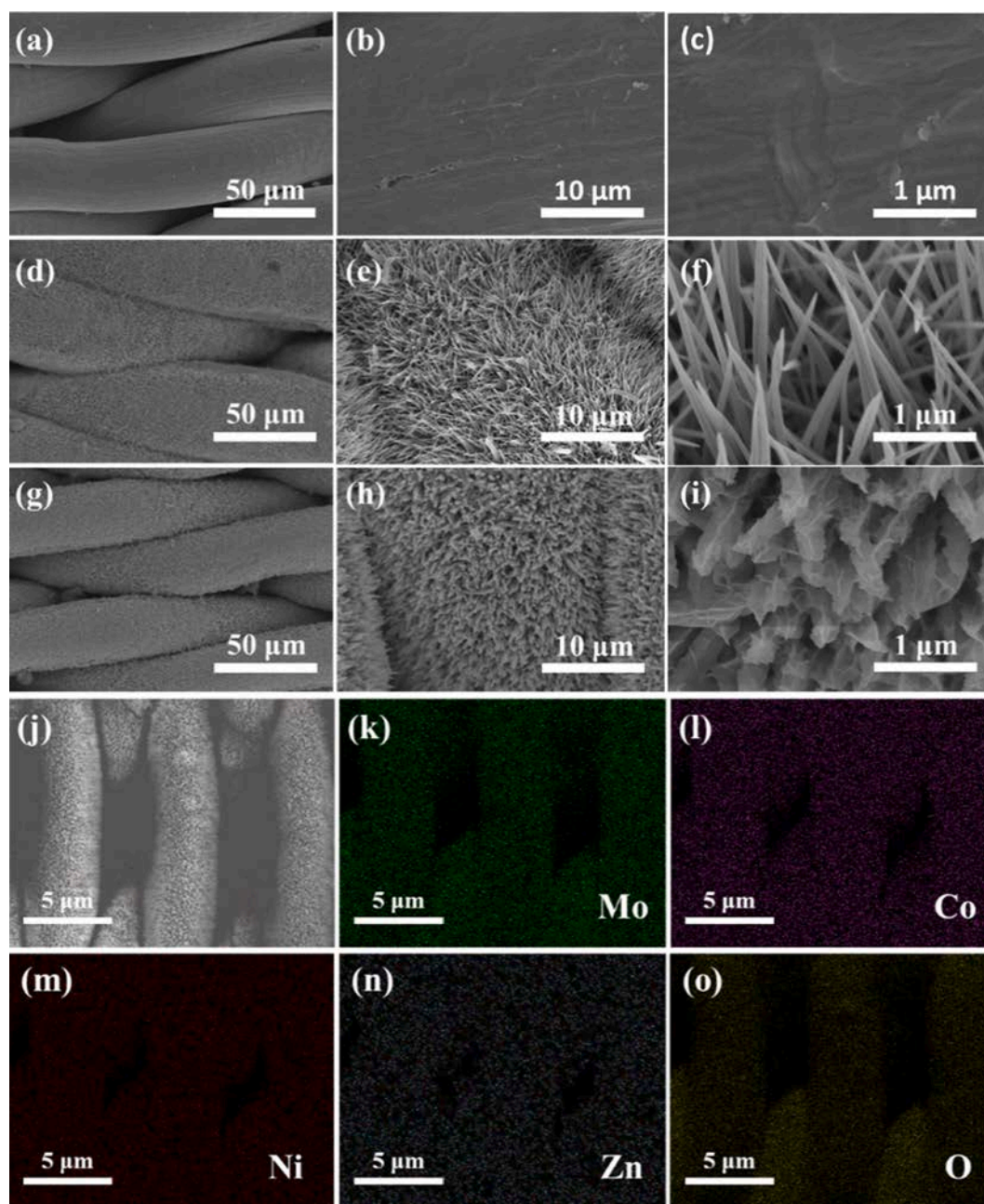
Fig. 2. SEM images of (a-c) the pristine SSM, (d-f) ZNC LDHs coated SSM and (g-i) ZNC@NM coated SSM at different magnification. (j) Selected area electron diffraction patterns of sample and (k-o) EDS spectrum of as-prepared heterojunction nanoarrays.

SSM substrates on the XRD peak signals, the powder samples prepared for XRD analysis were all scratched from the surface of SSM, where the microstructure of samples was relatively intact and remained constant with their microstructure on SSM (Fig. S3). After the first step of hy-drothermal reaction, we obtained the ternary multi-phase Zn-Ni-Co LDH with lattice defects. As was illustrated in Fig. 3, the peaks of Zn-Ni-Co LDH correspond to NiOOH (JCPDS 06–0075), Ni(OH)$_2$ (JCPDS 38–0715), Co(CO$_3$)$_{0.5}$(OH) (JCPDS 48–0083) and Zn$_5$(CO$_3$)(OH)$_6$ (JCPDS 19–1458) [38], indicating the formation of ternary LDH. The pure NiMoO$_4$ powder collected from the autoclave was assigned to the crystal texture standard card of PDF 00-012-0348. Comparing with the peaks of Zn-Ni-Co LDH, some new weak diffraction peaks were found in the XRD pattern of ZNC@NM due to the adhesion of NiMoO$_4$ nanosheets which corresponded to above standard PDF card [39–41]. Therefore, the results of XRD analysis confirmed the successful construction of

ZCM@NM nanoarrays.

To further investigate the chemical composition and valence states, XPS survey spectrum was performed as shown in Fig. 4a. It confirmed the existence of elements of Zn, Ni, Co, Mo and O on the surface of ZNC@NM-SSM, which was consistent with the results of EDS analysis. In the Zn 2p spectrum (Fig. 4b), two well-defined peaks were located at bind energy of 1021.2 eV (Zn 2p$_{3/2}$) and 1044.5 eV (Zn 2p$_{1/2}$), which was corresponded to the Zn (II) oxidation state in the hydroxide [38,42,43]. As displayed in Fig. 4c, the Ni 2p spectrum split into four main peaks at the bind energy 856. 4 eV, 861.45 eV, 873.6 eV and 880.1 eV, respectively. The fitted peaks observed at 856.4 eV and 873.6 eV corresponded to Ni 2p$_{3/2}$ and Ni 2p$_{1/2}$ accompanied by two satellite peaks and the spin-energy separation value was 17.2 eV, assigning to the Ni (II) oxidation state [38,43]. As was shown in Co 2p spectrum (Fig. 4d), the binding energy peaks located at 780.3 eV and 796 eV
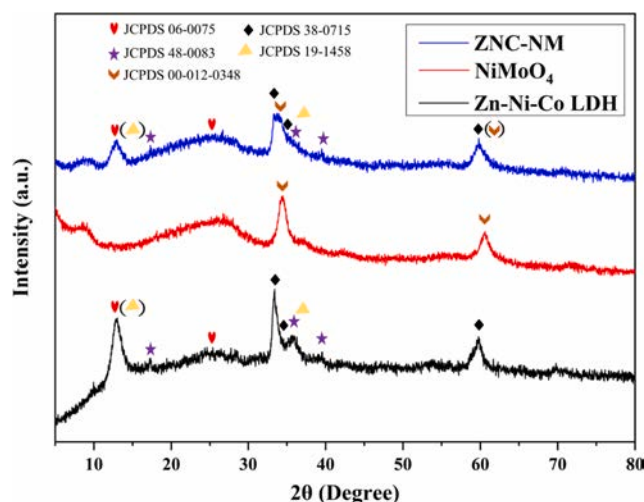
Fig. 3. XRD patterns of Zn-Ni-Co LDH, NiMoO$_4$ and ZNC@NM.

belonged to the Co^{2+} ions, while peaks situated in 775.2 eV and 792 eV were related to Co^{3+} [44–46]. Additionally, the Co 2p spectrum contained two region of Co 2p$_{3/2}$ and Co 2p$_{1/2}$ with the two shakeup distinct satellite peaks (787.6 eV and 802 eV) indicating the existence of Co^{2+} and Co^{3+}. In Mo 3d spectrum (Fig. 4e), two distinctive peaks located at the binding energy of 232.26 eV and 235.32 eV was assigned to the Mo 3d$_{3/2}$ and Mo 3d$_{5/2}$, which owned the separation of spin energy 3.06 eV, well confirming that elemental Mo exists as Mo^{6+} in NiMoO$_4$ [47]. Two fitted peaks in O 1 s spectrum (Fig. 4f) at 530.8 eV and 532.4 eV corresponded to the O^{2-} species in the lattice and the O-H from the structural or physisorbed water, respectively [43,48,49].

3.2. Wettability of the meshes

The wettability is mainly determined by the surface morphology and chemical composition of porous materials [50–52]. The static contact angle and dynamic absorption process were tested to evaluate the wetting behaviors of ZNC@NM-SSM. Fig. 5a showed that the pristine

SSM with smooth surface had a WCA of 100°. After the hydrothermal growth of ZNC LDH nanowires, the underwater oleophobicity of LDH coated SSM were greatly enhanced, with the underwater OCA of 143°. Further completing the construction of heterojunction nanoarrays, the underwater OCA and WCA of ZNC@NM-SSM were 164° and 0°, respectively, which demonstrated the superior water affinity of NiMoO$_4$. Additionally, high-speed photography system was conducted to measure the dynamic wetting behaviors of the ZNC@NM-SSM. In Fig. 5b, the water droplet was instantly absorbed within 0.24 s, exhibiting the outstanding superhydrophilicity of ZNC@NM nanoarrays. For efficient oil/water separation, we further explored the underwater wettability of ZNC@NM-SSM by immersing the coated mesh into water. After submerged, the water film forming on the surface of NiMoO$_4$ nanosheets would repel the oil and significantly reduced the contact area of oil/solid interface, resulting in low adhesion force. As was shown in the Fig. 6, all oils with underwater OCAs were greater than 150°, especially n-hexane with a contact angle up to 164.9°, demonstrating that ZNC@NM-SSMs owned distinctive underwater superoleophobicity. All the above results fully exhibited the feasibility and great potential of ZNC@NM-SSMs for oil/water separation.

3.3. Oil/water separation ability

To investigate the separation performance of ZNC@NM-SSMs, a series of oil/water mixtures (1:1 V/V) were tested to evaluate the separation capability. Considering the difference of oil density, two simple self-assembly devices driven by gravity without any external pressure were used to separate light oil and heavy oil, respectively (Fig. S4). Due to the repellence to oil of the coated mesh prewetted by water, the water phase rapidly penetrated the mesh into the collecting vessel, while the oil dyed with oil red was trapped above the mesh (Video S1). Fig. 7a-b illustrated the oil/water mixture before and after separation, respectively. After the oil/water mixtures were poured into the separation device, it could be observed that the water in the collecting container was transparent without any visible oil droplets.

Furthermore, the separation efficiency and filtration flux for various oils including petroleum, n-hexane, isooctane, kerosene, diesel and dichloromethane were calculated to quantitatively analyze the
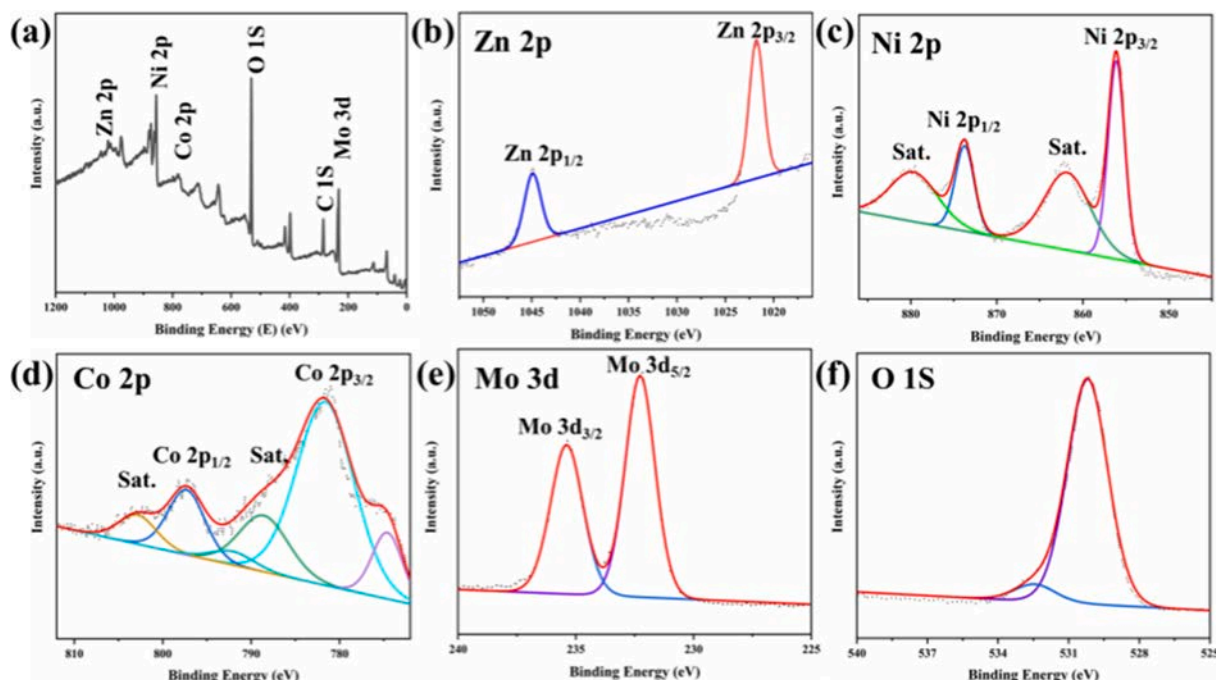

Fig. 4. XPS spectra of ZNC@NM-SSM (a) survey spectrum, (b) Zn 2p, (c) Ni 2p, (d) Co 2p, (e) Mo 3d and (f) O 1s.
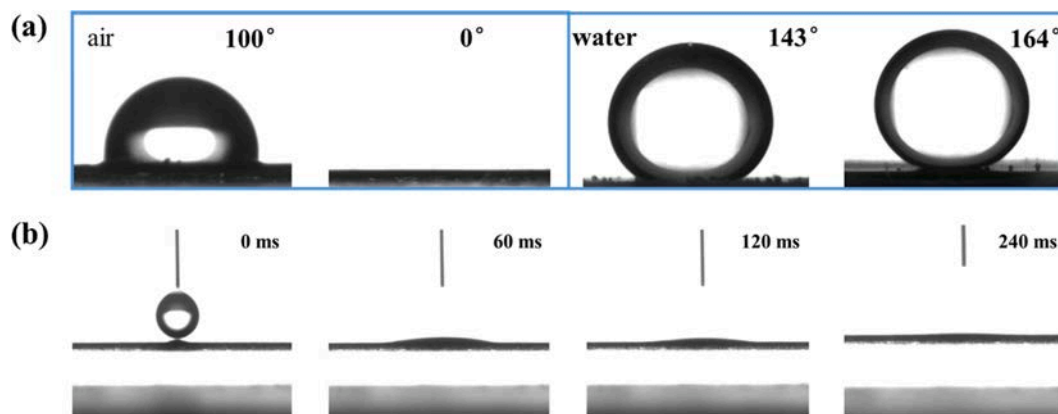
Fig. 5. (a) WCA of original SSM and ZNC@NM-SSM in the air, and underwater OCA of ZNC-SSM and ZNC@NM-SSM. (b) The dynamic absorption process of water droplet captured by a high-speed camera.
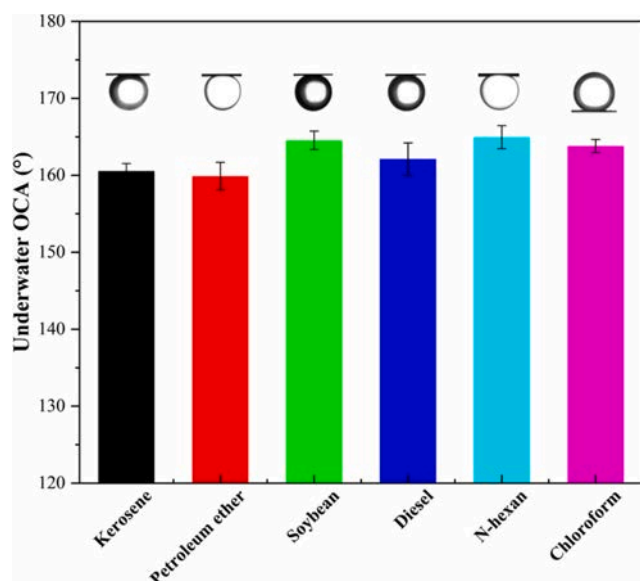

Fig. 6. The underwater OCA of various organic solvent.

separation performance of oil/water mixtures. As was seen in Fig. 8, the ZNC@NM-SSM exhibited ultrahigh separation efficiency, which were all in excess of 99.90%. Especially, the separation efficiency of dichloromethane/water mixture was as high as 99.98%. The water fluxes of six oil/water mixtures were all greater than 32,080 L m^{-2} h^{-1}. Moreover, water penetrated the coated mesh within 20 s for isooctane/water and petroleum/water mixtures. Therefore, the as-prepared coated mesh possessed favorable separation performance, which showed great prospect in the treatment of oily water. It was interesting that the water flux varied with different types of light oil/water mixtures due to the comprehensive effects of different density, viscosity, and interfacial tension [27,53,54]. Based on the Darcy's law, the permeability flux is directly proportional to the pressure and inversely proportional to the filtration resistance as well as the liquid viscosity [55]. For oil/water mixture of heavy oil, the separation device needs to be placed obliquely so that the water can maintain contact with the coating mesh to complete the oil-water separation process. As a consequence, the pressure of the oil-water mixture of the same volume in the inclined device is relatively small, resulting in a small flux.

In practical industrial applications, it was relatively difficult to separate emulsified oily wastewater due to oil or water droplets with different size were stably dispersed in the mixtures. Therefore, the separation of emulsions was of great necessity for evaluating separation performance of the coated mesh. Besides the separation of free oil /water mixtures, we also conducted the emulsion separation experiment to explore the separation performance of the ZNC@NM nanoarrays coated mesh. In this experiment, five sample oils containing petroleum ether, n-hexane, gasoline, diesel and dichloromethane were used to prepare oil-in-water emulsions. Fig. S5a, b illustrated the oil-in-water emulsions before and after separation, and the detailed separation process could be observed in the Video S2. In Fig. 9a, the micrograph of pre-separation and post-separation of oil-in-water emulsion illustrated that the milky white oil-in-water emulsion with average droplets size of 5–9 μm became clearly after passing through the equipment. Besides, it could be clearly observed from the image captured by an optical microscopy that there were no oil droplets in filtrate compared with the feed, indicating the successful separation of oil-in-water emulsion. To further evaluate the separation performance, separation efficiencies and permeation fluxes of emulsions were calculated. As shown in Fig. 9b, separation efficiencies for emulsions of petroleum ether-in-water, n-hexane-in-water, dichloromethane-in-water and diesel-in-water all exceeded 98% which were lower than those for the free oil/water mixtures due to the presence of tiny oil-in-water droplets dispersed in mixtures. In addition, the ZNC@NM coated mesh showed high permeation fluxes (e.g., permeation flux of petroleum ether-in-water reached up to 1981.60 L m^{-2} h^{-1}), indicating good separation performance for oily emulsions.

3.4. Recyclability and stability of the ZNC@NM-SSMs

The practical process of oil/water mixture separation often suffer from many harsh environments, so higher requirements are put forward for the recyclability and stability of oil-water separation materials. Therefore, we conducted the test of recyclability, mechanical stability, anti-corrosion and thermostability on the ZNC@NM-SSMs. The separation efficiency and flux for petroleum/water mixture were tested within 60 times to evaluate the recyclability, and every continuous separation of 10 times as a cycle was recorded. The ZNC@NM-SSMs was cleaned with anhydrous ethanol and dried at 80 °C after each separation. As shown in Fig. 10a, there was no significant change of separation efficiency, which still maintained above 99.9% within 60 times. Although the separation flux fluctuated slightly with the increasing number of separation, it remained at a high value. In addition, the SEM image and underwater OCA of the ZNC@NM-SSMs after 60-time recycles were measured to investigate the recyclability. In Fig. S6, although part of ZNC@NM nanoarrays on the front surface of SSM were destroyed slightly, the underwater OCA of the coated mesh was still higher than 150°, indicating the satisfactory recyclability of the ZNC@NM-SSMs.

In addition to the recyclability, mechanical stability is also one of the important factors affecting the long-term use of the ZNC@NM-SSMs duo
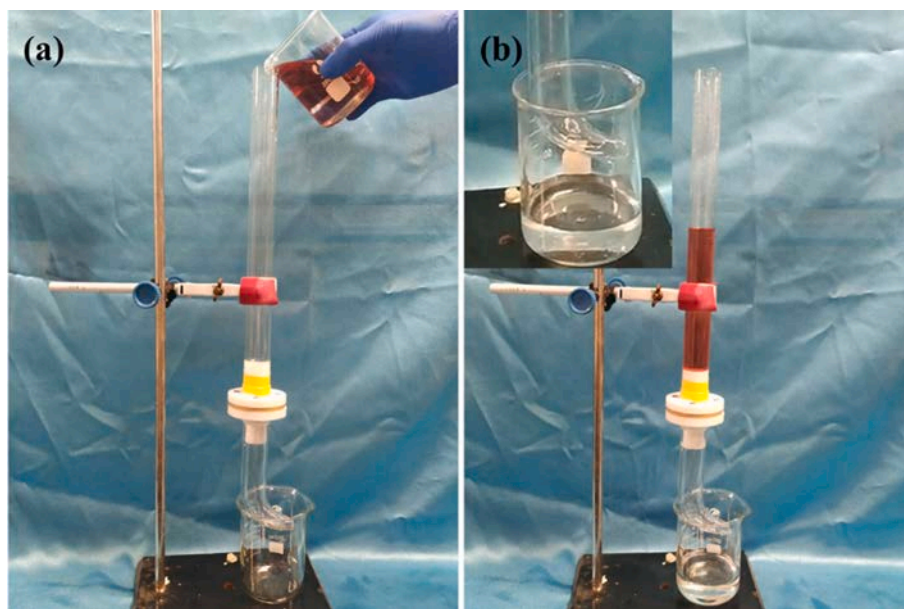
Fig. 7. Oil/water separation process of ZNC@NM-SSMs: (a) before separation, (b) after separation.
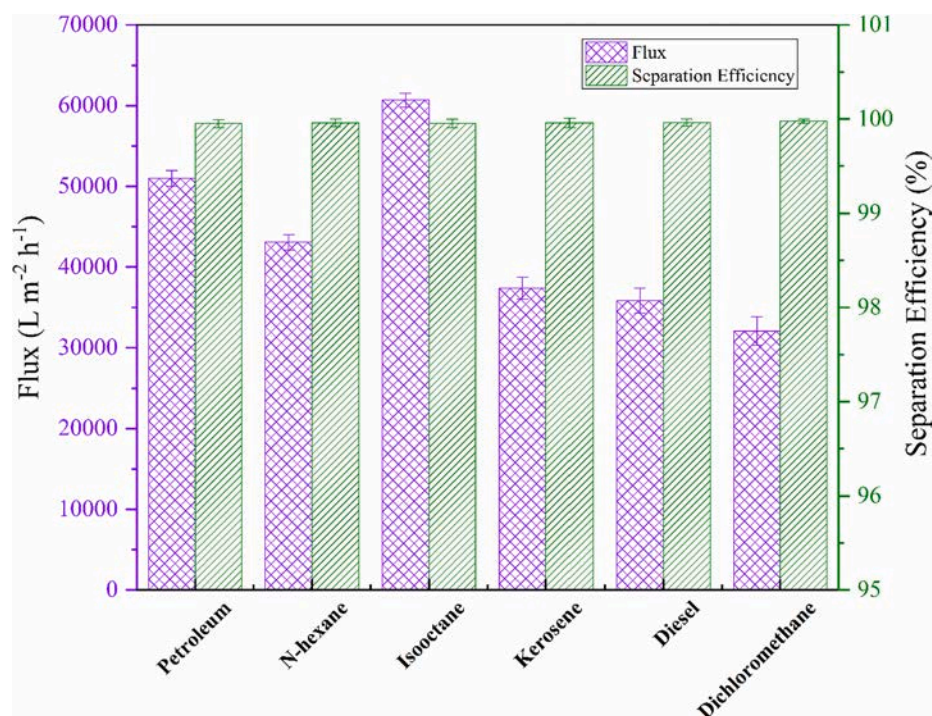

Fig. 8. Separation efficiency and permeation fluxes of various oil/water mixtures.

to the inevitable external force during the separation process. Therefore, we conducted the mechanical stability experiment by placing the coated mesh in an ultrasonic cleaning machine with powder of 50 W. Fig. 10b showed separation efficiency and underwater OCA of the ZNC@NM-SSMs with different ultrasonic time. Although separation efficiencies and underwater OCA decreased slightly with the increase of the ultrasonic time, they were still able to maintain separation efficiency of 99.13% and underwater OCA of 151.2° after 60 min of vibration. Besides, compared with the pristine microstructures, the tightly arrayed ZNC@NM nanoarrays treated by ultrasonic treatment could still be clearly observed, further demonstrated the good mechanical stability of ZNC@NM-SSMs (Fig. S7a-f).

Additionally, oily industrial wastewater with acidic/alkaline properties will destroy the surface microstructure of oil-water separation materials. For further investigating the chemical stability, the ZNC@NM-SSMs were immersed in an acidic/alkaline solution with various pH values from 2 to 14. After immersed for 24 h, the microtopography, underwater OCA and separation efficiency were measured to evaluate the anti-corrosive property of the as-prepared mesh. It can be clearly seen from the SEM image of Fig. S8a-g that the seagrass-like ZNC@NM nanoarrays of these samples soaked in solution (pH > 4) were still kept relatively intact, while NiMoO$_4$ nanosheets were etched relatively seriously in strong acidic solution (pH = 2), resulting in the exposure of ZNC LDHs. According to the results illustrated in Fig. 10c,
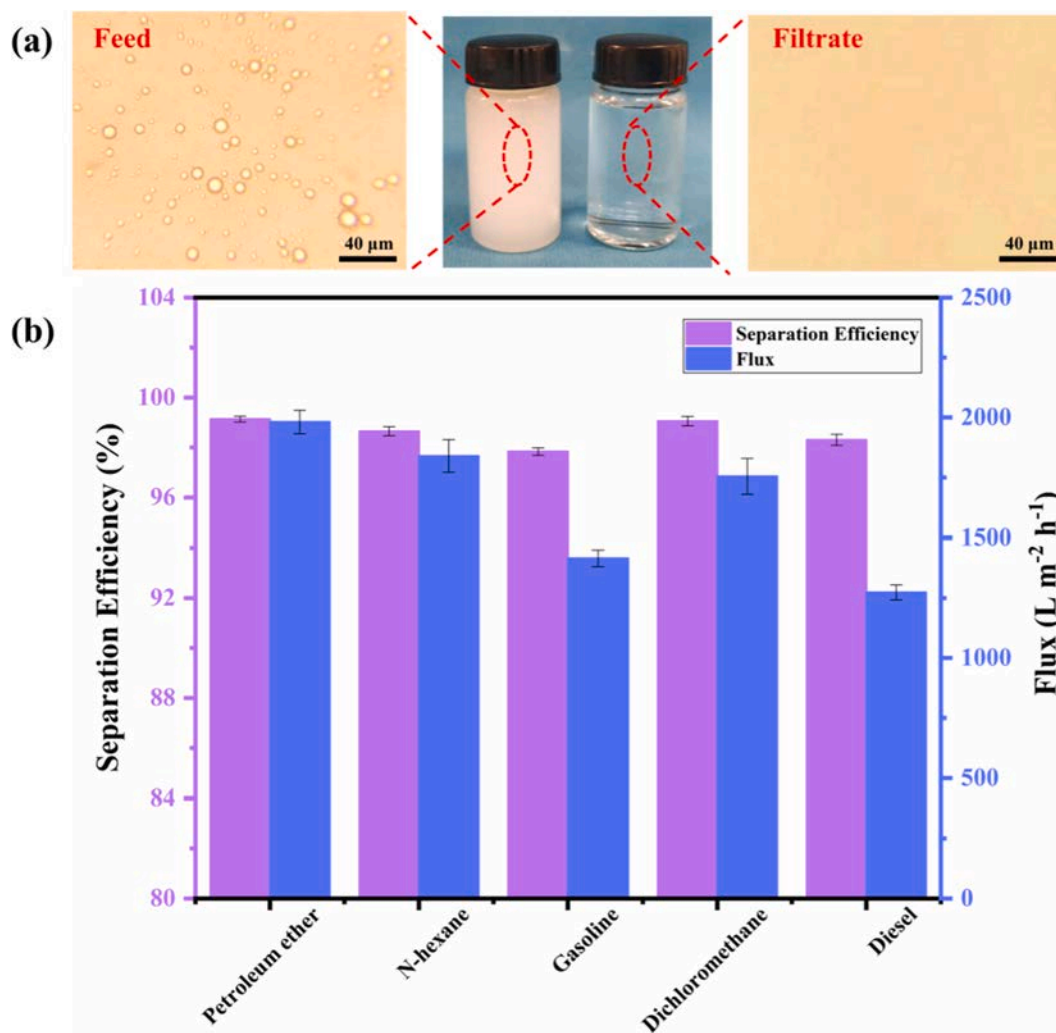
Fig. 9. (a) Photographs and micrographs of feed and filtrate. (b) Separation efficiency and permeation fluxes of various oil-in-water emulsions.

the ZNC@NM-SSMs remained underwater superoleophobicity with underwater OCA exceeding 150° and high separation efficiency above 98.54% in the acidic/alkaline solution (pH > 2), demonstrating that the ZNC@NM nanoarrays coated SSM owned good anti-corrosive property and could maintain high separation efficiency in a wide range of pH.

In general, functional materials with promising applications are required to withstand high temperature environments in order to cope with complex industrial conditions. In this paper, a series of tests were carried out on the ZNC@NM-SSMs treated at different temperatures for 4 h, and the thermal stability was explored by measuring the underwater oil contact and microscopic morphology after calcination. SEM of the ZNC@NM-SSMs revealed that the microstructure was not destroyed when calcination temperature was below 500 °C, indicating the favorable thermal stability of heterojunction nanoarrays coatings (Fig. 11a-e). As the temperature rose to 600 °C (Fig. 11f), $NiMoO_4$ nanosheets turn into serrated structure due to minor damage caused by high temperature. Beyond that, there were no significant variations of the underwater OCA, which remained above 160° as shown in Fig. 10d, further demonstrating great thermal stability of the as-prepared coated mesh. More significantly, the coated mesh can realize self-cleaning at high temperature by utilizing its thermal stability. In Fig. S9, the ZNC@NM-SSM polluted by oleic acid solution (oleic acid: ethyl alcohol = 1:9, m/m) with the WCA of 58.8° recovered its superhydrophilicity after calcination at 350 °C for 1 h.

3.5. Anti-fouling property and self-cleaning performance

In the process of oil/water separation, the material will inevitably be polluted by oil, which greatly restricts the long-term service life. Therefore, anti-fouling property and self-cleaning performance are especially important in practical application. Based on this, we conducted three different experiments to investigate oil resistance and self-cleaning behavior of the ZNC@NM-SSM. Fig. 12a depicted that the engine oil (dyed with oil red) attaching on the prewetting ZNC@NM-SSM slid completely, leaving clean surface when it was rinsed with water. In Fig. 12b, the engine oil was ejected onto the surface of ZNC@NM-SSM underwater with a syringe, and the oil droplets instantly bounced off the surface, floating to the water without any adhesion. After completing the process of injecting machine oil underwater, the ZNC@NM-SSM was immersed into and lifted out of the water repeatedly. It was found that there was no oil droplets on its surface, while the tweezers surface contaminated by red oil was as a contrast (Fig. 12c). All the above tests showed that the as-prepared ZNC@NM-SSM exhibited satisfactory anti-fouling property and underwater self-cleaning performance, which was contribute to prolong its service life in oily wastewater.

3.6. Photocatalytic performance of the mesh

With the development of modern industry, the composition of wastewater is increasingly complex, which often contains different
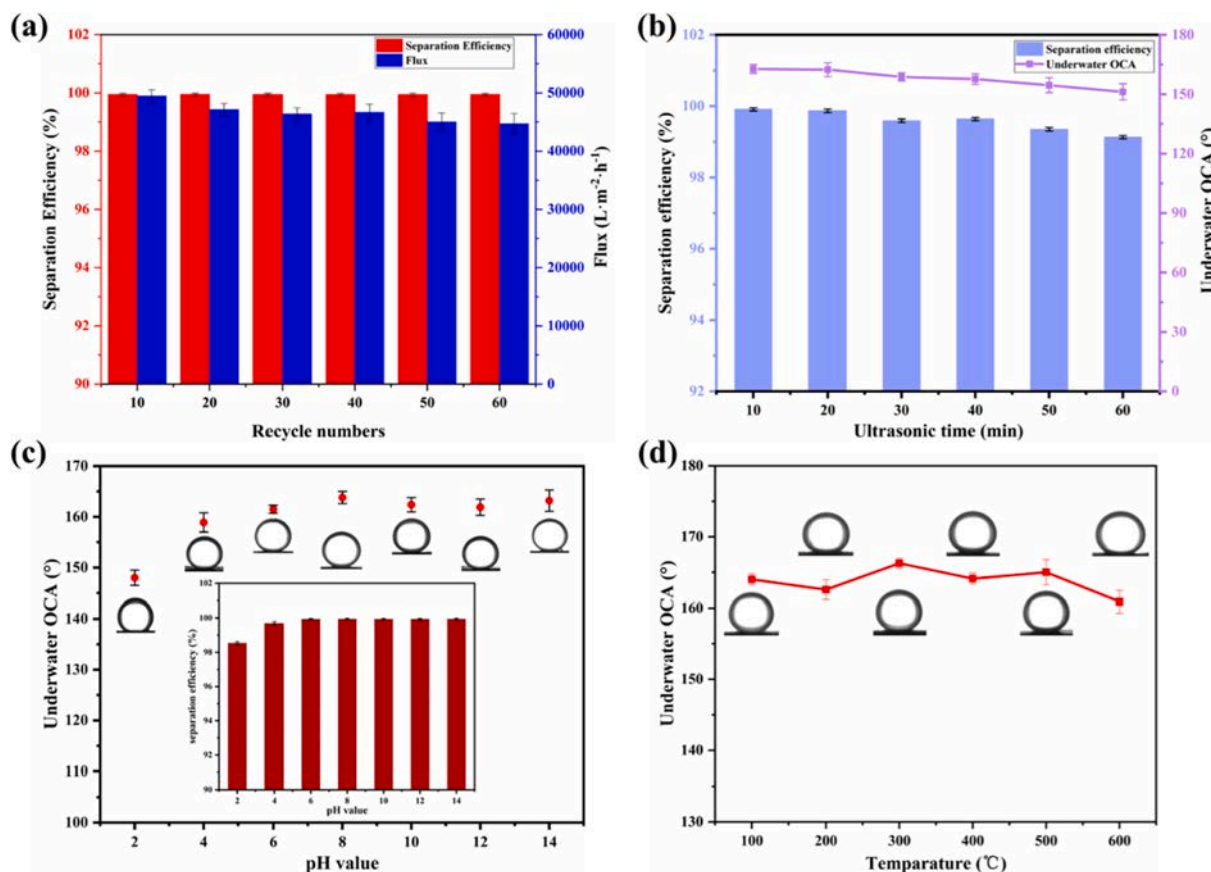
Fig. 10. (a) Separation efficiency and permeation flux of petroleum/water mixture for repeated use. (b) The separation efficiency and underwater OCA after different ultrasonic time. (c) Underwater OCA and separation efficiency of ZNC@NM-SSMs after immersed in acidic/alkaline solution. (d) The change of underwater OCA of different samples calcined at different temperatures.
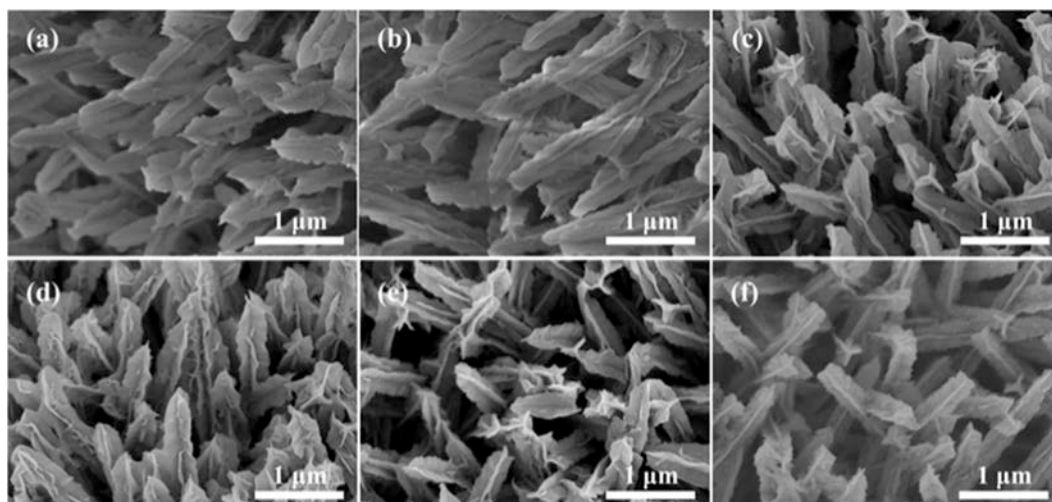

Fig. 11. SEM image of the ZNC@NM-SSMs calcined at 100 °C, 200 °C, 300 °C, 400 °C, 500 °C and 600 °C, respectively (a-f).

kinds of organic dyes. It has been proven an effective method to degrade the organic dyes in wastewater with photocatalyst. To investigate the photocatalytic performance of the ZNC@NM-SSM, UV–vis spectrophotometer was used to measure the solution absorbance curve of CR and MB during the photo-degradation process. As shown in Fig. 13a, the absorbance intensities of CR solution at 501 nm was gradually decreased with the increasing of the visible light irradiation time, indicating the concentration of CR solution reduced constantly. By comparing the

insert images before and after irradiation, it could be clearly observed that the solution nearly became colorless after 150 min of irradiation. Moreover, MB aqueous solution tended to be transparent more quickly in Fig. 13c. To further quantitatively analyze the photocatalytic efficiency of the prepared coated mesh, the standard curve of the dyes was fitted to calculate the degradation efficiency (Fig. S10). The kinetic plot of C/C_0 of all samples under the same condition for CR solution and MB solution was represented (Fig. 13b, d). After exposed to visible light for
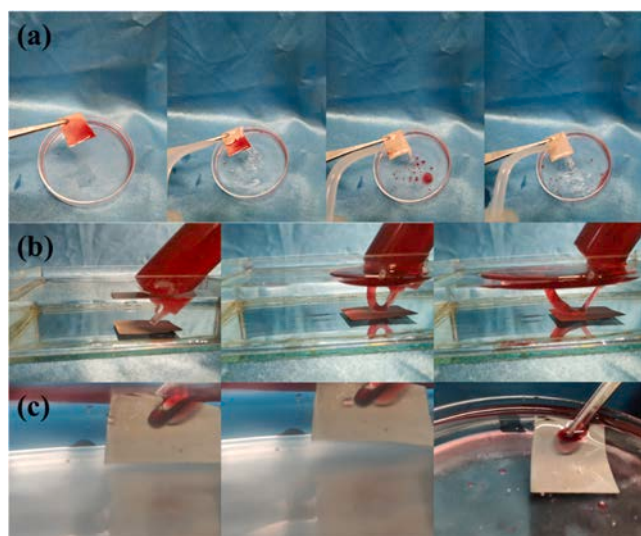
Fig. 12. Self-cleaning property and underwater anti-fouling of ZNC@NM-SSM: (a) Prewetting ZNC@NM-SSM polluted by engine oil dyed with oil red was rinsed with water. (b) Engine oil dyed with oil red was injected on the surface of ZNC@NM-SSM. (c) Move the ZNC@NM-SSM wetted by water in polluted engine oil/water mixture repeatedly.

150 min, the degradation rate of CR solution for ZNC@NM-SSM, ZNC-SSM and pristine mesh were 89.99%, 65.47% and 3.3%, respectively, and the self-degradation of CR was below than 5% in the control experiment (Fig. 13b). In addition, the degradation rate of the coated

mesh for MB solution reached to 93.95% within 80 min (Fig. 13d). **Table S1** presented a comparison of dye degradation efficiency of some reported membranes in the literature and ZNC@NM-SSMs in this work. As was observed, the ZNC@NM nanoarrays on the SSM had higher capacity to degrade dyes in visible light than $BiVO_4$, $CuWO_4@Cu_2O$ and GTP aerogel. In addition, the as-prepared heterojunction nanoarrays with visible light responsiveness enhanced the utilization rate of solar energy compared with $MnMoO_4$ coated mesh and TiO_2 coated fabric, which could only absorb 4% ultraviolet light of the solar spectrum. It is well known that many reports in literatures fabricated photocatalytic materials with precious metals to enhanced photocatalytic performance. Compared with those photocatalytic materials in literatures, the ZNC@NM-SSM was fabricated with relatively low-cost ingredients, while its photocatalytic performance was not inferior to precious metals [56–58]. Based on the above analysis, the design of ZNC@NM heterostructure nanoarrays endow it good photocatalytic performance for the purification of the organic dyes in wastewater. Moreover, as a dual-functional material, the ZNC@NM-SSM has a broad application prospect in the fields of wastewater treatment and photocatalysis due to its chemical stability, nontoxic, high temperature resistance and high catalytic efficiency.

The superhydrophilicity of the ZNC@NM-SSM is conducive to the contact of dye aqueous solution with the surface of heterostructure nanoarrays, thus enhancing its photocatalytic performance [59]. Compared with pure $NiMoO_4$, the response of composite heterojunction nanoarrays to visible light is also enhanced [34,60,61]. The schematic representation of the photocatalysis mechanism is shown in the Fig. 14. Under the irradiation of visible light, electron-hole pairs (e_{CB}^-/h_{VB}^+) with high activity are generated and migrate to the surface of ZNC@NM due to the absorption of phonon energy. Subsequently, O_2 and H_2O absorbed
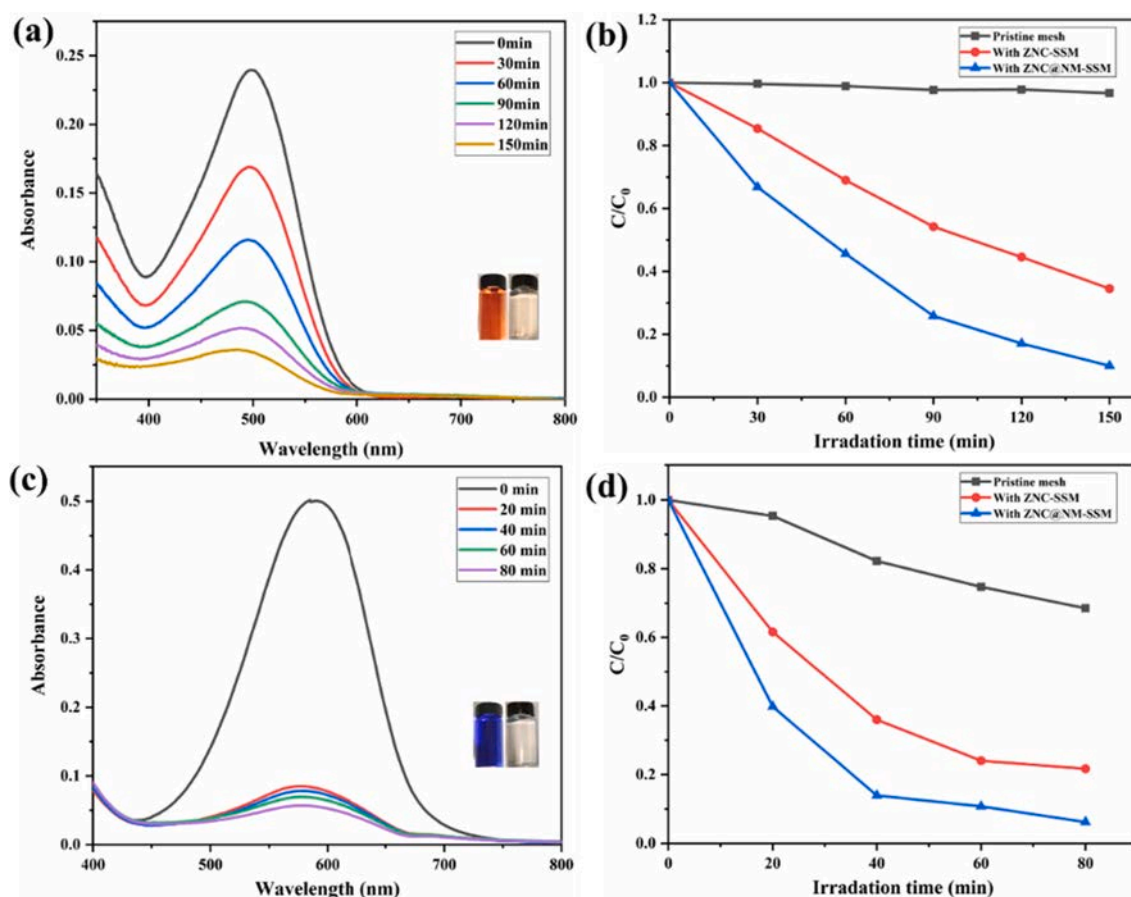

Fig. 13. (a) The absorbance curve of CR during the photodegrade process. (b) Degradation rate of the pristine mesh, ZNC-SSM and ZNC@NM-SSM to CR solution. (c) The absorbance curve of MB during the photodegrade process. (d) Degradation rate of the pristine mesh, ZNC-SSM and ZNC@NM-SSM to MB solution.
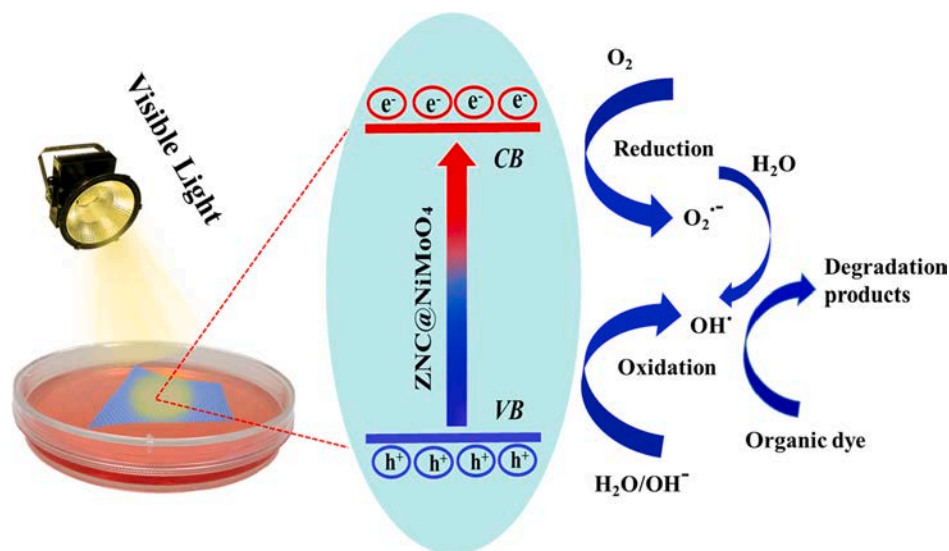
Fig. 14. Photocatalytic degradation mechanism schematic of ZNC@NM heterostructure nanoarrays.

on the surface of heterostructure nanoarrays react with electron-hole pairs and are transformed to a mass of superoxide radical ($O_2^{\bullet-}$) and hydroxyl radical ($OH^{\bullet}$), which all have super oxidizing capacity, especially the $OH^{\bullet}$ that can react with organic dyes directly. Therefore, the as-prepared coated mesh can efficiently degrade dyes for wastewater remediation.

4. Conclusion

In summary, we have successfully fabricated a superhydrophilic seagrass-like nanoarrays on the surface of SSM with great photocatalytic capacity via a facile two-step hydrothermal method. Super-hydrophilicity and hydration ability were realized by construct $NiMoO_4$ nanosheets on ternary Zn-Ni-Co LDH nanowires with high underwater OCA of 164.9°, which facilitated the achievement of high permeation flux of 60,674 $L \cdot m^{-2} \cdot s^{-1}$ and ultrahigh efficiency of 99.98% for free oil/ water mixtures. The satisfactory self-cleaning and anti-fouling property ensured the prepared mesh with the separation efficiency exceeding 99.9% within 60 recycles. Moreover, The ZNC-NM coated mesh polluted by contamination could recover original underwater OCA by annealing at 350 °C and still remained superhydrophilicity after immersed in solution with a series of pH from 2 to 14. The formation of heterojunction structure on the SSM greatly reduced the recombination rate of electron-hole pairs of $NiMoO_4$, which could effectively degrade dyes and organic pollution. Consequently, the dual-functional coated mesh possesses broad application prospects and it is expected to be a competitive candidate in fields of oily wastewater treatment and photocatalytic degradation.

CRediT authorship contribution statement

Yongli Sun: Validation, Supervision, Project administration, Funding acquisition. **Jingshuai Li:** Conceptualization, Methodology, Software, Validation, Formal analysis, Investigation, Resources, Data curation, Writing - original draft, Writing - review & editing, Visualization, Supervision, Project administration. **Luhong Zhang:** Validation, Supervision, Project administration, Funding acquisition. **Bin Jiang:** Validation, Supervision, Project administration, Funding acquisition. **Xiaodong Yang:** Software, Validation, Writing - review & editing. **Na Yang:** Validation, Writing - review & editing, Supervision. **Feifei Peng:** Supervision. **Mi Xu:** Supervision. **Xiaoming Xiao:** Validation, Supervision, Project administration, Funding acquisition.

Declaration of Competing Interest

The authors declare that they have no known competing financial interests or personal relationships that could have appeared to influence the work reported in this paper.

Appendix A. Supplementary data

Supplementary data to this article can be found online at https://doi.org/10.1016/j.seppur.2020.118116.

References

[1] Z. Gong, N. Yang, Z. Chen, B. Jiang, Y. Sun, X. Yang, L. Zhang, Fabrication of meshes with inverse wettability based on the TiO₂ nanowires for continuous oil/ water separation, Chem. Eng. J. 380 (2020).

[2] W. Li, Q. Meng, X. Li, C. Zhang, Z. Fan, G. Zhang, Non-activation ZnO array as a buffering layer to fabricate strongly adhesive metal-organic framework/PVDF hollow fiber membranes, Chem. Commun. 50 (2014) 9711–9713.

[3] X. Liu, L. Ge, W. Li, X. Wang, F. Li, Layered double hydroxide functionalized textile for effective oil/water separation and selective oil adsorption, ACS Appl. Mater. Interfaces 7 (2015) 791–800.

[4] B. Bolvardi, J. Seyfi, I. Hejazi, M. Otadi, H.A. Khonakdar, S.M. Davachi, Towards an efficient and durable superhydrophobic mesh coated by PDMS/TiO₂ nanocomposites for oil/water separation, Appl. Surf. Sci. 492 (2019) 862–870.

[5] P.-C. Chen, Z.-K. Xu, Mineral-coated polymer membranes with superhydrophilicity and underwater superoleophobicity for effective oil/water separation, Sci. Rep. 3 (2013) 2776.

[6] M. Nikkhah, T. Tohidian, M.R. Rahimpour, A. Jahanmiri, Efficient demulsification of water-in-oil emulsion by a novel nano-titania modified chemical demulsifier, Chem. Eng. Res. Des. 94 (2015) 164–172.

[7] Y. Jiang, H. Qi, X. Zhang, Novel method for separation and screening of lubricant-degrading microorganisms and bacterial biodegradation, Chin. J. Chem. Eng. 24 (2016) 353–359.

[8] L. Feng, S. Li, Y. Li, H. Li, L. Zhang, J. Zhai, Y. Song, B. Liu, L. Jiang, D. Zhu, Superhydrophobic surfaces: from natural to artificial, Adv. Mater. 14 (2002) 1857–1860.

[9] L. Zhang, X. Yang, B. Jiang, Y. Sun, Z. Gong, N. Zhang, S. Hou, J. Li, N. Yang, Superhydrophilic and underwater superoleophobic Ti foam with robust nanoarray structures of TiO₂ for effective oil-in-water emulsion separation, Sep. Purif. Technol. 252 (2020).

[10] Z. Shami, S.M. Amininasab, P. Shakeri, Structure-property relationships of nanosheeted 3D hierarchical roughness MgAl-layered double hydroxide branched to an electrospun porous nanomembrane: a superior oil-removing nanofabric, ACS Appl. Mater. Interfaces 8 (2016) 28964–28973.

[11] X. Yue, J. Li, T. Zhang, F. Qiu, D. Yang, M. Xue, In situ one-step fabrication of durable superhydrophobic-superoleophilic cellulose/LDH membrane with hierarchical structure for efficiency oil/water separation, Chem. Eng. J. 328 (2017) 117–123.

[12] L. Zhang, Z. Gong, B. Jiang, Y. Sun, Z. Chen, X. Gao, N. Yang, Ni-Al layered double hydroxides (LDHs) coated superhydrophobic mesh with flower-like hierarchical structure for oil/water separation, Appl. Surf. Sci. 490 (2019) 145–156.

[13] S. Lu, Y. Zhao, X. Hu, Y. Lin, Y. Ke, Biomimetic fabrication of micron/nano-meter assembled superhydrophobic polymer fiber fabrics for oil/water separation, Mater. Lett. 262 (2020).

[14] Y. Wang, M. Dugan, B. Urbaniak, L. Li, Fabricating nanometer-thick simultaneously oleophobic/hydrophilic polymer coatings via a photochemical approach, Langmuir 32 (2016) 6723–6729.

[15] W. Zhang, N. Liu, Y. Cao, Y. Chen, Q. Zhang, X. Lin, R. Qu, H. Li, L. Feng, Polyacrylamide-polydivinylbenzene decorated membrane for sundry ionic stabilized emulsions separation via a facile solvothermal method, ACS Appl. Mater. Interfaces 8 (2016) 21816–21823.

[16] X. Bai, Z. Zhao, H. Yang, J. Li, ZnO nanoparticles coated mesh with switchable wettability for on-demand ultrafast separation of emulsified oil/water mixtures, Sep. Purif. Technol. 221 (2019) 294–302.

[17] J. Wang, F. Han, Y. Chen, H. Wang, A pair of MnO_2 nanocrystal coatings with inverse wettability on metal meshes for efficient oil/water separation, Sep. Purif. Technol. 209 (2019) 119–127.

[18] Y. Gong, J. Huang, L. Cao, K. Kajiyoshi, D. Yang, Y. Feng, L. Kou, L. Feng, Methanol-assisted synthesis of Ni^{3+}-doped ultrathin NiZn-LDH nanomeshes for boosted alkaline water splitting, Dalton Trans. 49 (2020) 1325–1333.

[19] J. Cui, Z. Zhou, A. Xie, Q. Wang, S. Liu, J. Lang, C. Li, Y. Yan, J. Dai, Facile preparation of grass-like structured NiCo-LDH/PVDF composite membrane for efficient oil-water emulsion separation, J. Membr. Sci. 573 (2019) 226–233.

[20] L. Mohapatra, K. Parida, A review on the recent progress, challenges and perspective of layered double hydroxides as promising photocatalysts, J. Mater. Chem. A 4 (2016) 10744–10766.

[21] J. Li, Y. Xu, Z. Ding, A.H. Mahadi, Y. Zhao, Y.-F. Song, Photocatalytic selective oxidation of benzene to phenol in water over layered double hydroxide: a thermodynamic and kinetic perspective, Chem. Eng. J. 388 (2020).

[22] P. Gholami, A. Khataee, R.D.C. Soltani, L. Dinpazhoh, A. Bhatnagar, Photocatalytic degradation of gemifloxacin antibiotic using Zn-Co-LDH@biochar nanocomposite, J. Hazard. Mater. 382 (2020) 121070.

[23] Q.-K. Lei, Q. Zhang, X.-Y. Wu, X. Wei, J. Zhang, K.-X. Wang, J.-S. Chen, Towards ultra-stable lithium metal batteries: Interfacial ionic flux regulated through LiAl LDH-modified polypropylene separator, Chem. Eng. J. 395 (2020).

[24] S. Zhang, Z. Liu, D. Chen, Z. Guo, M. Ruan, Oxygen vacancies engineering in TiO_2 homojunction/ZnFe-LDH for enhanced photoelectrochemical water oxidation, Chem. Eng. J. 395 (2020).

[25] S. Dong, Y. Wang, J. Li, D. Zhang, Y. Zhou, Y. Tong, Tuning the crosslink structure of cationic hydrogel for enhanced chromium(VI) removal: the covalent and electrostatic co-crosslinked effects and adsorption mechanism, Chem. Eng. J. 394 (2020).

[26] K. Wang, C. Miao, Y. Liu, L. Cai, W. Jones, J. Fan, D. Li, J. Feng, Vacancy enriched ultrathin TiMgAl-layered double hydroxide/graphene oxides composites as highly efficient visible-light catalysts for CO_2 reduction, Appl. Catal. B-Environ. 270 (2020).

[27] Y. Xie, Y.H. Gu, J. Meng, X. Yan, Y. Chen, X.J. Guo, W.Z. Lang, Ultrafast separation of oil/water mixtures with layered double hydroxide coated stainless steel meshes (LDH-SSMs), J. Hazard. Mater. 398 (2020) 122862.

[28] W. Lv, Q. Mei, J. Xiao, M. Du, Q. Zheng, 3D Multiscale superhydrophilic sponges with delicately designed pore size for ultrafast water separation, Adv. Funct. Mater. 27 (2017).

[29] D. Cui, R. Zhao, J. Dai, J. Xiang, F. Wu, A hybrid $NiCo_2O_4$@$NiMoO_4$ structure for overall water splitting and excellent hybrid energy storage, Dalton Trans. 388 (2020).

[30] V.T. Chebrolu, B. Balakrishnan, S. Aravindha Raja, H.J. Kim, A facile synthesis of a $NiMoO_4$@metal-coated graphene-ink nanosheet structure towards the high energy density of a battery type-hybrid supercapacitor, Dalton Trans. (2020).

[31] X. Li, J. Xu, X. Zhou, Z. Liu, Y. Li, S. Zhao, L. Li, M. Mao, Amorphous CoS modified nanorod $NiMoO_4$ photocatalysis for hydrogen production, J. Mater. Sci.-Mater. Electron. 31 (2019) 182–195.

[32] S. Peng, L. Li, H.B. Wu, S. Madhavi, X.W.D. Lou, Controlled growth of $NiMoO_4$ nanosheet and nanorod arrays on various conductive substrates as advanced electrodes for asymmetric supercapacitors, Adv. Energy Mater. 5 (2015).

[33] S. Kumar Ray, D. Dhakal, G. Gyawali, B. Joshi, A. Raj Koirala, S. Wohn Lee, Transformation of tetracycline in water during degradation by visible light driven Ag nanoparticles decorated $α-NiMoO4$ nanorods: Mechanism and pathways, Chem. Eng. J. 373 (2019) 259-274.

[34] S.K. Ray, D. Dhakal, S.W. Lee, Rapid degradation of naproxen by $AgBr-α-NiMoO_4$ composite photocatalyst in visible light: mechanism and pathways, Chem. Eng. J. 347 (2018) 836–848.

[35] S.K. Ray, D. Dhakal, S.W. Lee, Insight into malachite green degradation, mechanism and pathways by morphology-tuned alpha-$NiMoO_4$ photocatalyst, Photochem. Photobiol. 94 (2018) 552–563.

[36] J. Low, J. Yu, M. Jaroniec, S. Wageh, A.A. Al-ghamdi, Heterojunction photocatalysts, Adv. Mater. 29 (2017).

[37] C. Wu, J. Cai, Q. Zhang, X. Zhou, Y. Zhu, P.K. Shen, K. Zhang, Hierarchical mesoporous Zinc-Nickel-Cobalt ternary oxide nanowire arrays on nickel foam as high-performance electrodes for supercapacitors, ACS Appl. Mater. Interfaces 7 (2015) 26512–26521.

[38] Z.-H. Huang, F.-F. Sun, M. Batmunkh, W.-H. Li, H. Li, Y. Sun, Q. Zhao, X. Liu, T.-Y. Ma, Zinc-nickel-cobalt ternary hydroxide nanoarrays for high-performance supercapacitors, J. Mater. Chem. A 7 (2019) 11826–11835.

[39] P. Bandyopadhyay, G. Saeed, N.H. Kim, J.H. Lee, Zinc-nickel-cobalt oxide@ $NiMoO_4$ core-shell nanowire/nanosheet arrays for solid state asymmetric supercapacitors, Chem. Eng. J. 384 (2020).

[40] M. Wiesmann, H. Ehrenberg, G. Wltschek, P. Zinn, H. Weitzel, H. Fuess, Crystal structures and magnetic properties of the high-pressure modifications of $CoMoO_4$ and $NiMoO_4$, J. Magn. Magn. Mater. 150 (1995) L1–L4.

[41] J.L. Brito, J. Laine, Detection of $β-NiMoO_4$ in oxidic nickel-molybdenum catalysts, Appl. Catal. 72 (1991) L13–L15.

[42] E. Raphael Ezeigwe, L. Dong, J. Wang, L. Wang, W. Yan, J. Zhang, MOF-deviated zinc-nickel-cobalt ZIF-67 electrode material for high-performance symmetrical coin-shaped supercapacitors, J. Colloid Interface Sci. 574 (2020) 140–151.

[43] W. Hu, H. Wei, Y. She, X. Tang, M. Zhou, Z. Zang, J. Du, C. Guo, D. Bao, Flower-like nickel-zinc-cobalt mixed metal oxide nanowire arrays for electrochemical capacitor applications, J. Alloy. Compd. 708 (2017) 146–153.

[44] C. Guan, X. Liu, W. Ren, X. Li, C. Cheng, J. Wang, Rational design of metal-organic framework derived hollow $NiCo_2O_4$ arrays for flexible supercapacitor and electrocatalysis, Adv. Energy Mater. 7 (2017).

[45] Y.-R. Liu, X. Shang, W.-K. Gao, B. Dong, X. Li, X.-H. Li, J.-C. Zhao, Y.-M. Chai, Y.-Q. Liu, C.-G. Liu, In situ sulfurized CoMoS/CoMoO₄ shell-core nanorods supported on N-doped reduced graphene oxide (NRGO) as efficient electrocatalyst for hydrogen evolution reaction, J. Mater. Chem. A 5 (2017) 2885–2896.

[46] S. Wen, T. Yang, N. Zhao, L. Ma, E. Liu, Ni-Co-Mo-O nanosheets decorated with NiCo nanoparticles as advanced electrocatalysts for highly efficient hydrogen evolution, Appl. Catal. B-Environ. 258 (2019).

[47] J. Guo, X. Zhang, Y. Sun, L. Tang, X. Zhang, Self-template synthesis of hierarchical $CoMoS_3$ nanotubes constructed of ultrathin nanosheets for robust water electrolysis, J. Mater. Chem. A 5 (2017) 11309–11315.

[48] Y. Zeng, Z. Lai, Y. Han, H. Zhang, S. Xie, X. Lu, Oxygen-vacancy and surface modulation of ultrathin nickel cobaltite nanosheets as a high-energy cathode for advanced Zn-ion batteries, Adv Mater. (2018) e1802396.

[49] H. Xia, G. Li, H. Cai, X. Li, P. Sun, P. Wang, J. Huang, L. Wang, D. Zhang, Y. Yang, J. Xiong, Interlaced NiMn-LDH nanosheet decorated $NiCo_2O_4$ nanowire arrays on carbon cloth as advanced electrodes for high-performance flexible solid-state hybrid supercapacitors, Dalton Trans. 48 (2019) 12168–12176.

[50] Y. Zhang, H. Wang, B. Liu, X. Zhao, Y. Wei, $NiCo_2O_4$ hierarchical structure coated mesh with long-term stable underwater superoleophobicity for high-efficient, high-flux oil-water separation, Appl. Surf. Sci. 504 (2020).

[51] C. Chen, D. Weng, A. Mahmood, S. Chen, J. Wang, Separation mechanism and construction of surfaces with special wettability for oil/water separation, ACS Appl. Mater. Interfaces 11 (2019) 11006–11027.

[52] X.J. Feng, L. Jiang, Design and creation of superwetting/antiwetting surfaces, Adv. Mater. 18 (2006) 3063–3078.

[53] J. Dai, L. Wang, Y. Wang, S. Tian, X. Tian, A. Xie, R. Zhang, Y. Yan, J. Pan, Robust nacrelike graphene oxide-calcium carbonate hybrid mesh with underwater superoleophobic property for highly efficient oil/water separation, ACS Appl. Mater. Interfaces 12 (2020) 4482–4493.

[54] A. Xie, J. Cui, J. Yang, Y. Chen, J. Dai, J. Lang, C. Li, Y. Yan, Photo-Fenton self-cleaning membranes with robust flux recovery for an efficient oil/water emulsion separation, J. Mater. Chem. A 7 (2019) 8491–8502.

[55] J. Wang, X. Wang, S. Zhao, B. Sun, Z. Wang, J. Wang, Robust superhydrophobic mesh coated by PANI/TiO_2 nanoclusters for oil/water separation with high flux, self-cleaning, photodegradation and anti-corrosion, Sep. Purif. Technol. 235 (2020).

[56] C. Xu, W. Lu, M. Li, Y. Cao, H. Pang, C. Gong, S. Cheng, Trifunctional copper mesh for integrated oil/water separation, SERS detection, and pollutant degradation, ACS Appl. Mater. Interfaces 6 (2019).

[57] Z. Zhang, Y. Yang, C. Li, R. Liu, Porous nanofibrous superhydrophobic membrane with embedded Au nanoparticles for the integration of oil/water separation and catalytic degradation, J. Membr. Sci. 582 (2019) 350–357.

[58] B. Kwon Kaang, N. Han, W. Jang, H. Young Koo, Y. Boo Lee, W. San Choi, Crossover magnetic amphiprotic catalysts for oil/water separation, the purification of aqueous and non-aqueous pollutants, and organic synthesis, Chem. Eng. J. 331 (2018) 290–299.

[59] L. Ma, J. He, J. Wang, Y. Zhou, Y. Zhao, Y. Li, X. Liu, L. Peng, M. Qu, Functionalized superwettable fabric with switchable wettability for efficient oily wastewater purification, in situ chemical reaction system separation, and photocatalysis degradation, ACS Appl. Mater. Interfaces 11 (2019) 43751–43765.

[60] S.M. Ghoreishian, G. Seeta Rama Raju, E. Pavitra, C.H. Kwak, Y.-K. Han, Y.S. Huh, Controlled synthesis of hierarchical α-nickel molybdate with enhanced solar-light-responsive photocatalytic activity: A comprehensive study on the kinetics and effect of operational factors, Ceram. Int. 45 (2019) 12041-12052.

[61] S.K. Ray, D. Dhakal, Y.K. Kshetri, S.W. Lee, Cu-α-$NiMoO_4$ photocatalyst for degradation of Methylene blue with pathways and antibacterial performance, J. Photochem. Photobiol. A-Chem. 348 (2017) 18–32.